PROCEEDINGS OF SPIE

SPIEDigitalLibrary.org/conference-proceedings-of-spie

Plasmonic nanopore sensing with continuous AC modulation

Scott Renkes, Minjun Kim, George Alexandrakis

Scott Renkes, Minjun Kim, George Alexandrakis, "Plasmonic nanopore sensing with continuous AC modulation," Proc. SPIE 12649, Optical Trapping and Optical Micromanipulation XX, 1264905 (5 October 2023); doi: 10.1117/12.2680254

SPIE.

Event: SPIE Nanoscience + Engineering, 2023, San Diego, California, United States

Plasmonic Nanopore Sensing with Continuous AC Modulation

Scott Renkes*[a], Minjun Kim[b], George Alexandrakis[a]
[a]University of Texas at Arlington, Bioengineering Department, Arlington, TX, USA
[b]Southern Methodist University, Department of Mechanical Engineering, Dallas, TX, USA

ABSTRACT

The use of plasmonic nanopores for single molecule detection has attracted considerable attention due to their high sensitivity and selectivity. In this study, we present a phase analysis approach for characterizing the trapping of single molecules in an AC-driven plasmonic nanopore. By analyzing the phase response of the plasmonic nanopore at select frequencies, we can differentiate between a test ligand, the antibody targeting this ligand, and the complexes that these ligands form, as well as observe their dynamics while inside the optical trap of the plasmonic nanopore. This pilot work shows the feasibility of a new approach for rapid and accurate identification of single molecules in complex mixtures.

Keywords: plasmonic, nanopores, nanoparticles, AC modulation, SANE sensor

1. INTRODUCTION

Nanopores are commonly used to discriminate between analytes through the analysis of changes in conduction current profiles during translocation. Nanopore measurements have enabled discrimination between single molecule species in solution[1] and attained low-cost and label-free DNA sequencing [2,3] with additional possible applications expanding rapidly.[4,5] However, the translocation times of analytes through a traditional nanopore are extremely fast, which limits the fidelity of electrical data that can be collected. Through the use of optical trapping enabled by the self-induced back-action (SIBA) effect, nanopores can be enhanced not only by slowing down the translocation of analytes, but also by introducing new dimensionality to the collected data through the collection of optical data simultaneously with electrical data.[6,7] To that end, we previously developed a SIBA actuated nanopore electrophoresis (SANE) sensor, effectively a nanopore with plasmonic optical trapping, which has been shown to be capable of trapping individual nanoparticles (NPs), proteins and protein complexes[8] and, through the use of bimodal optical and electrical data, can discriminate between analyte species.[6,9,10]

We can collect additional information on trapped analytes by driving the SANE sensor with a constant AC voltage. In contrast to a triggered burst of short-duration AC signals,[11] here we propose a constant AC voltage to ensure the AC voltage is applied to the analyte at the instant it enters and leaves the trap. Furthermore, we can then decompose the frequency response into real and imaginary components to analyze phase shifts that can occur at the instant of trapping as well as phase shifts that can occur while trapped and after the analyte leaves the trap. This work presents the application of a constant AC signal to optical trapping experiments with peptide-major histocompatibility complex (pMHC) and targeted antibodies to examine the potential benefits for improved analyte identification as compared to previous work on burst AC analyses applied to the same analytes.[9]

2. EXPERIMENTAL SETUP

For these experiments we use the SANE sensor,[12] which is a plasmonic nanopore utilizing a double nanohole (DNH) shaped nanoantenna the resonates broadly in the near-infrared (NIR) range.[13] To induce optical trapping, we illuminate the plasmonic nanoantenna with a linearly polarized 820 nm continuous wave (CW) laser diode (L820P200, Thorlabs, Newton, NJ). A quarter wave plate, followed by a Glan-Thompson polarizer and a half-wave plate, allowed us to orient the linearly polarized light produced by the laser diode to the narrow waist of the SANE sensor, as seen in Fig. 1. The laser beam was expanded to overfill the back side of our 1.2 NA C-Apochromat water immersion objective lens (Zeiss). This gave us a rough spot size of 500 μm and a focal optical power of ~20 mW. Optical transmission data from the sensor was captured by a photodiode (Thorlabs, Newton, NJ), as shown in Fig. 1. The quarter wave plate was intentionally misaligned in both yaw and pitch in order to reduce light being trapped in the return beam path, due to the highly reflective gold surface of the sensor, which would create unpredictable intensity fluctuations at the laser

*sar9179@mavs.uta.edu; phone 1 740 272-6710

Optical Trapping and Optical Micromanipulation XX, edited by Kishan Dholakia, Gabriel C. Spalding, Proc. of SPIE Vol. 12649, 1264905 · © 2023 SPIE
0277-786X · doi: 10.1117/12.2680254

diode. The output of the diode was connected to an Axopatch 200B (Molecular Devices, San Jose, CA) to enable synchronous collection with electrical data, as described below.

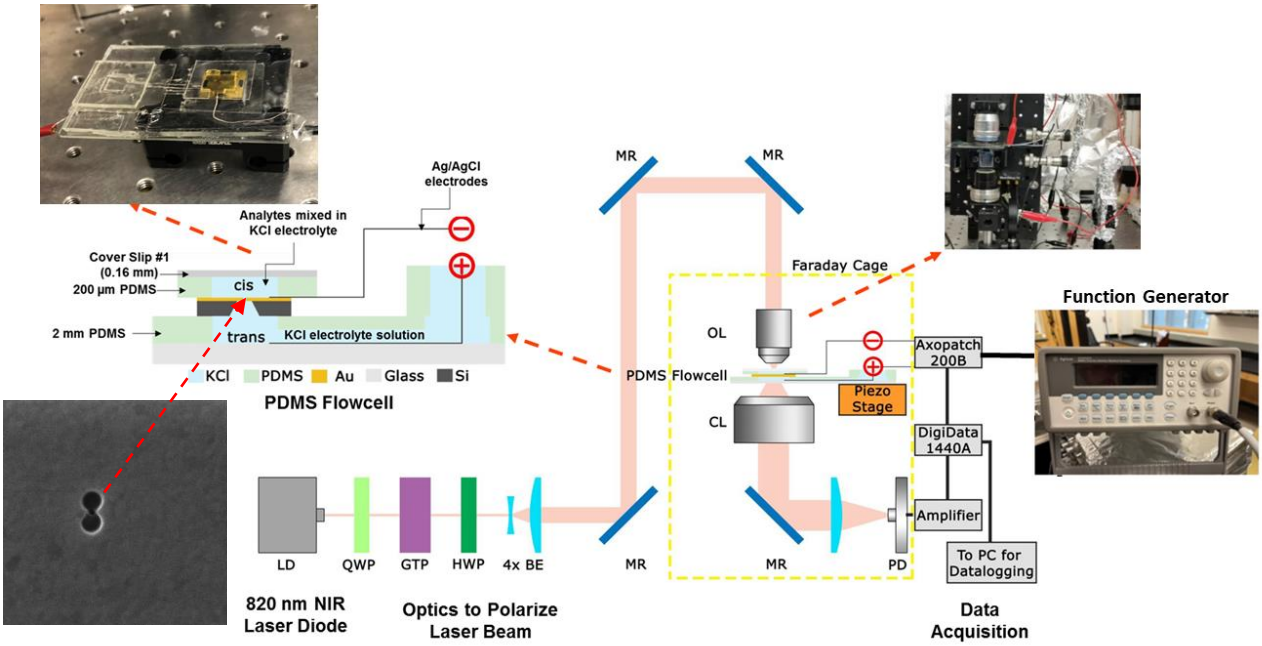

Figure 1: Experimental Setup

For the electrical signal sensing, we employed an Axopatch 200B to serve as a voltage clamp, to establish our AC signal and 100 mV DC electrophoretic voltage, as well as an amplifier. The Axopatch 200B had an adjustable Bessel filter with a maximum cutoff frequency of 100 kHz, which limited the range of available AC frequencies to test. The maximum AC frequency we used in these experiments was 80 kHz. Ag/AgCl low noise electrodes were used to connect the Axopatch Headstage to our flow cell. To digitize the collected electrical signals we used a Digidata 1550B (Molecular Devices) that had a maximum sampling rate of 500 kHz and subsequently data was recorded using the pClamp software. The AC signal was driven using a function generator (33250A Agilent, Santa Clara, CA) operated in sine wave mode without a trigger.

To process the collected optical and electrical data, we exported the Axon Binary File (ABF), a proprietary data format managed by Molecular Devices, into Matlab (MathWorks, Natick, MA). The data was then segmented by detecting the leading and trailing edges of the optical trap data, which usually presented with a step-like feature in their time-series data. The height of the optical step was measured as well as the electrical pulse amplitude upon both trapping and trap exiting, and the time between those two instances was also quantified (trap duration). These parameters were stored in a database and the segmented data was stored as a blob in the Azure cloud. Using this method allowed for better aggregation of data and quicker recall of trapping events in subsequent analyses.

Once the data was segmented, we recalled each trap and filtered the AC command voltage and signal response using an infinite impulse response (IIR) notch filter using the Matlab filter creator function. The IIR notch filter had a center frequency equal to the AC command voltage, 1 kHz in this case, and ± 3% bandwidth around this AC frequency. Both the filtered and unfiltered data were converted to complex numbers using the Hilbert transform. A delta-phase between the command voltage and resulting electrical signal phases was calculated by the Hilbert transform of both the IIR-filtered electrical signal and IIR-filtered command voltage. The resulting instantaneous complex number was used to calculate the phase angles (φ) and the difference between the φs defined delta-phase ($\Delta\varphi$). We then took the gradient of this $\Delta\varphi$, plotted it over time and compared it with the raw optical and filtered electrical signal traces. We examined both the raw and filtered $\Delta\varphi$ gradients and determined it was easier to visually discern features in the filtered data. We also opted to unwrap the phase to account for a phase velocity that was present in all of our data. Furthermore, we explored using the Hilbert-Huang transform (HHT), continuous wavelet transform

(CWT), and short time Fourier transform (SFTF) to extract phase information but yielded little additional information from our cursory analysis.

Finally, for the data analysis, we used the Matlab fit() function, with the Levenberg-Marquart parameter selected, to fit a damped oscillation superimposed to a steady state sine wave. This was accomplished by further segmenting the data based on the leading edge of the optical trap to capture the first peak of the trapping spike and then terminating the data segment at +0.5 ms to ensure the steady state oscillatory component did not dominate our data fitting.

For analytes, we used H-2Db RAH antigen (RAH), a major histocompatibility complex (MHC) class I allotype from c57Blk/6 (mouse strain) analogous to human leukocyte antigen (HLA) consisting of a purified mouse MHC I heavy chain, H-2Db (35 kDa) and a human b2m (13 kDa) light chain. RAHYNIVTF(49-57) (1 kDA) derived from human papilloma virus-16 (HPV) E7 protein was loaded onto the RAH antigen by *in vitro* refolding to create a peptide-presenting MHC (pMHC) antigen.[14] An antibody, targeted to the RAH, which we call anti-RAH (150 kDa) was generated by classical B cell hybridoma technology.[15] Isolates of the RAH and anti-RAH were run through the sensor at various concentrations ranging from 1 aM to 1 pM. An equimolar solution was created by first combining the analytes at ~100 nM concentration and left to incubate for 20 minutes to allow for a bound fraction to develop at a higher concentration. The incubated solution was used in the experiments in titrations from 1 aM to 1 pM at 1 order of magnitude increments.

3. OVERVIEW OF OPTICAL AND AC ELECTRICAL SENSOR SIGNALS

Figures 2a and 2b show three data traces corresponding to (1) the optical transmission through the sensor (red), (2) the filtered electrical signal (orange) using an IIR notch filter, and (3) the gradient of the sensor's electrical signal with time (purple). The collected optical data showed step changes at the time that trapping occurs, with the heighth of that step being roughly proportional to the volume of the analyte (RAH, anti-RAH, or complex). The filtered electrical signal had the profile of a damped oscillation, which we fit to an empirical formula to extract electrical signal parameters to help discriminate between analytes, as discussed below. A small fraction of the AC command voltage amplitude leaked past the IIR filter and into the electrical signal, most likely because the empty SANE sensor was also found to be sensitive to transient electrical responses for AC voltages in the 1-10 kHz range. Finally, $\Delta\varphi$ was plotted as a gradient with time to make smaller scale features of potential interest more clearly visible, relative to the much larger absolute magnitude of those signals.

By observing the phase gradient traces in Figs. 2a and 2b, one can see that there is a sharp phase change as the analyte enters the optical trap. On either side of the trapping event, there was a reduction in the RMS variability of the $\Delta\varphi$ gradient signal. This leads us to believe that in the absence of an analyte near the optical trap, there was very little contribution of the phase component of the HHT, which created higher noise in the deduced $\Delta\varphi$ signal. As the analyte approached the sensor, however, it dominated the phase signal, which reduced the signal's RMS variability. The analyte ceased to dominate the phase once it came to rest in the optical trap. The RMS signal variability increased again as charge motions in the conducting Au layer reduced significantly when the moving charge of the analyte had come to rest. A mirror of this $\Delta\varphi$profile was seen when the analyte left the trap and translocated through the underlying nanopore (not shown). Additionally, we observed a periodicity to the RMS envelope of the phase outside of the trapping event that correlates with the driving AC signal, likely due to AC command signal leak past the notch filter. This can be corrected in future work by fine-tuning the notch filter. However, we have also confirmed that there is a second phase gradient spike, post-trap, that does not occur in step with the periodic AC signal. This is confirmed by comparing Figs. 2a and 2b, that show signals in the ~1.8 kHz range (initial dip in the range curves), independent of the command voltage frequencies.

We explored other methods of extracting phase components of the signal to get a better idea of long-term phase shifts, but the time domain analyses revealed a large phase velocity that dominated the signal. This masked the phase shift we expected to see. Kitta et. al.[16] showed the $\Delta\varphi$ in traditional nanopores to be in millidegrees. In future work, we will either employ a lock-in amplifier or adjust our phase calculation method to get down to that level of precision.

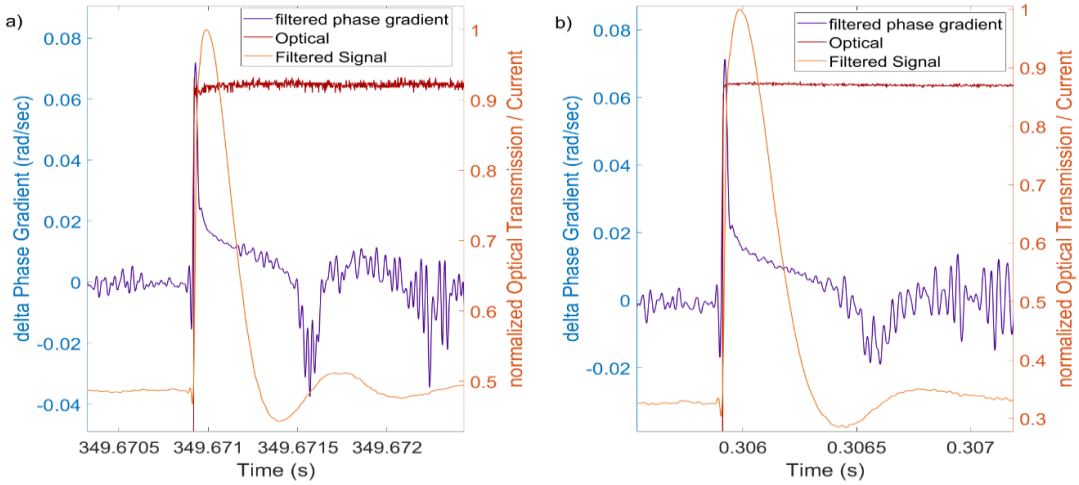

Figure 2:a) Plots for a likely complex (1k Hz). b) Plot for RAH (50k Hz).

4. EXTRACTING ANALYTE PARAMETERS FROM POST-TRAPPING TRANSIENT ELECTRICAL SIGNALS

As found in our previous experiments,[11] we can fit a damped oscillation to a pulsed AC signal that can provide electrical signatures of the analyte(s) near or inside the trap. We have followed the same logic here but have added a constant AC signal term (Eq. 1) to reflect the experimental conditions relevant to this work. In addition to a constant AC term, Eq. 1 contains the damped oscillation term, a DC offset and linear baseline correction for drift:

$$Eq1: y = a_1 + a_2 * x + b_1 * \sin(c_1 * x - d_1) * e^{e_1 * x} + b_2 * \sin(c_2 * x - d_2)$$

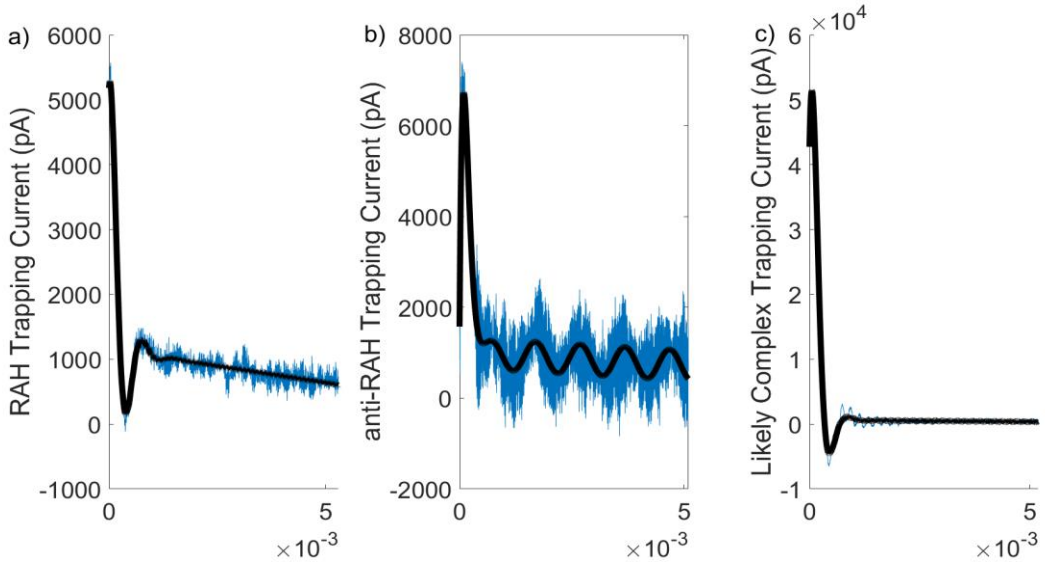

Figure 3: a) Fitted decay of RAH. b) Fitted decay of anti-RAH. c) Fitted decay of likely complex.

We fitted three traces representing the three analyte types encountered in our experiments: RAH (Fig. 3a), anti-RAH (Fig. 3b) and likely complexes formed in equimolar solutions of RAH and anti-RAH (Fig. 3c). We have also

noted the presence of much smaller electrical signals accompanied by short-lived optical traps (not shown), which are likely peptides that either fell out of the RAH protein pocket into which they are designed to bind, or protein fragments not fully separated during sample purification. A few events with large-size optical and electrical signatures were also detected, likely corresponding to agglomerates. It was also noted that the anti-RAH data had a higher noise floor compared to other experiments in this set, which may have resulted in worse fits. We will work on identifying the reason for this noise in near-future work.

The six parameters we could extract from curve-fitting Eq. 1 were the DC offset, a1; linear correction, a2; damped oscillation magnitude, b1; natural frequency, c1; phase of the natural frequency, d1; and the exponential decay, e1. Figure 4 shows each parameter derived from the corresponding three traces in Fig. 3. Parameters a1, a2, and b1 are likely impacted by the size and charge of the molecule. Also, the decay magnitude, b1, likely represent ions displaced by the molecule entering the trap and then mirrored by the conducting gold layer. Larger molecules, or complexes, have more surface area to hold charge and have a shallower decay. This is represented by the exponential decay, e1, as the electrical signal returns to steady state. Although these initial results suggest that frequency of the damped oscillation, c1, is largely independent of the driving AC frequency, it is still not clear what the relative contribution of other analytes packed near the sensor contributes to the overall electrical signal. We will address this question in future work by performing analyte titrations at ever-lower concentrations.

Cursory observation of the panels in Fig. 6 indicates the distinct possibility of separating analytes by fitting the post-trapping electrical damped oscillation data. In near-future work, we will aggregate more traces to test the statistical significance of these findings, as we have done previously for AC burst data.[11]

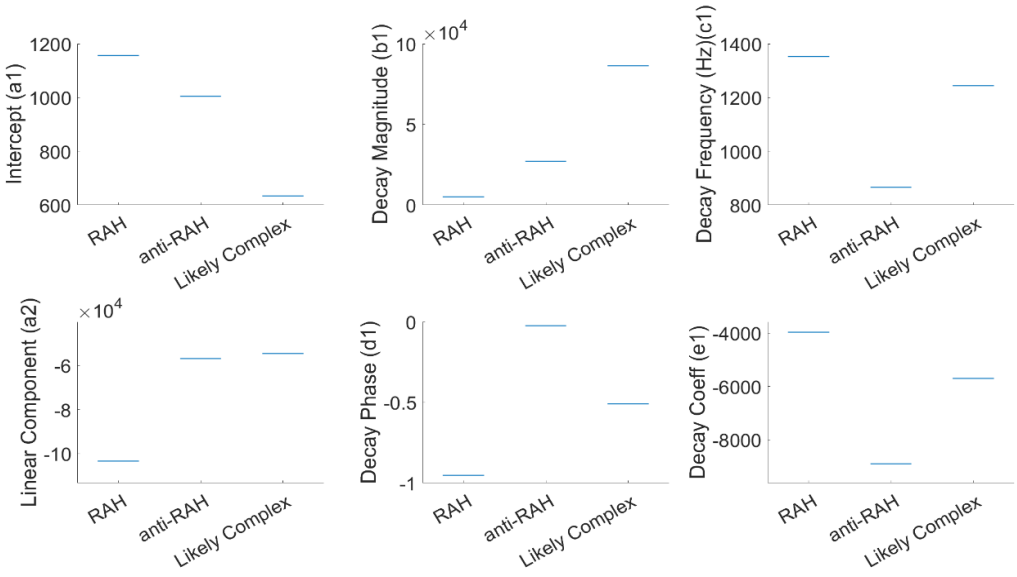

Figure 4: Parameters fitted to Eq. 1 for RAH, anti-RAH and likely RAH-anti-RAH complex.

5. ADDITIONAL POST-TRAPPING OPTICAL-ELECTRICAL DATA FEATURES

While analyzing time-series data of trapping events, a trend became apparent where distinct smaller-size steps, relative to the initial trapping event, occurred typically within milliseconds after the trapping initiation. The much smaller amplitude of these signal relative to typical trapping event amplitudes[10] invited an alternate explanation. Upon closer inspection, we saw corresponding electrical signal changes that were synchronous to those optical events. Figure 5a shows the most commonly observed occurrence after trapping events, which indicated a small step down in optical transmission concurrent with a minor dip in electrical current. This occurred in 70% of cases out of 177 events

analyzed. Figure 5b shows an example of a much less common (~16%) step-up event in optical transmission that was more prevalent for the smaller analyte, RAH, and at higher AC frequencies (>10 kHz). For completeness, we note that in the remaining ~14% of cases there was no detectable small optical step.

We hypothesize that both optical step-up and step-down phenomena can be explained by considering the detailed light intensity hotspot profile at the mouth of this plasmonic nanopore sensor. Specifically, our prior work has indicated the existence of two optical intensity hotspots within few nanometers of the sharp edge of the DNH Au tips.[17] The gap

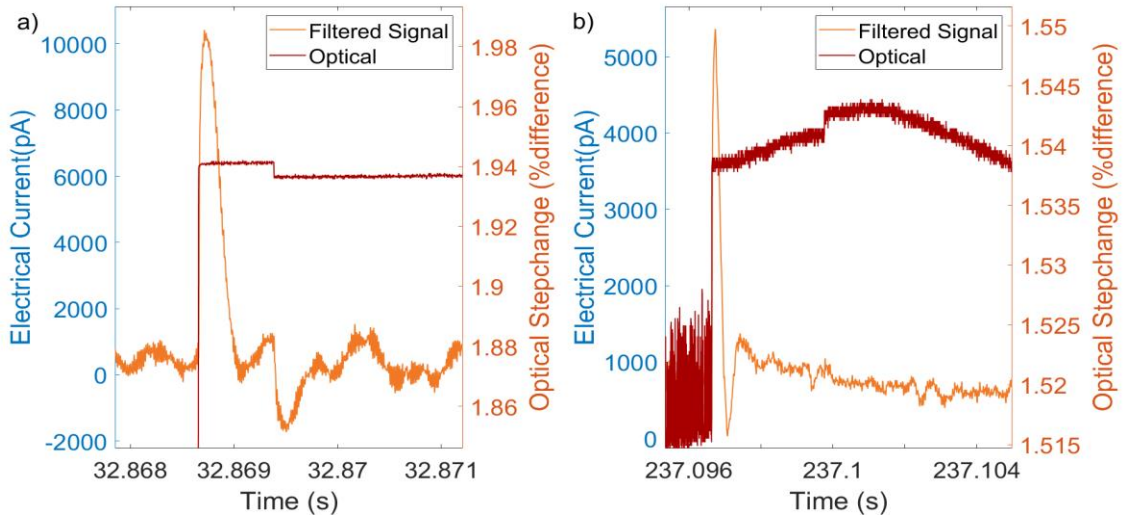

Figure 5: a) Possible trapping into a single hotspot near an Au DNH tip (likely complex, 1k Hz). b) Possible trapping between two hotspots (RAH, 10k Hz).

between Au tips is ~30 nm (Fig. 1) and as a result, a lower intensity area is formed at the center of this optical trap immediately above the center of the underlying electrical nanopore. It is important to note that the optical signal is created by optical scattering of the analyte being trapped by the SIBA mechanism, which attracts the analyte towards the highest light intensity regions.[18] It is conceivable that an analyte is initially attracted to the center of the SANE sensor because that is where the highest electrophoretic and electrostatic forces exist.[17] However, shortly thereafter, the analyte finds a more stable trapping location in one of the two optical hotspots on either side of the narrow waist of the DNH. When an analyte in the immediate vicinity of the Au tips of the DNH, the light that it scatters couples into a plasmon and we would expect the transmitted intensity to reduce, as in the step-down event seen in Fig. 3a. As the two light hotspots are the most stable trapping locations, this could explain why these step-down events are the most common occurrence for all analytes. In addition, the optical step-down signal was synchronous with a distinct dip in electrical signal (orange curve in Fig. 5a). The latter is consistent with a charged analyte's movement from the center towards the edges of the optical trap, where the increased proximity to the Au tips would induce electrical transients to equalize charges. Following this argument, when an analyte is pushed from one of the two light hotspots towards the center of the trap, as we presume occurs in Fig. 5b, a step increase in transmitted optical intensity would be expected because there is less scattered light coupled into the Au tip plasmons. It is reasonable then to expect that this occurrence would be less frequent as the center of the optical trap is a secondary minimum for trapping stability. It would also make sense that the smaller analytes, RAH in this case, would be more vulnerable to be pushed by electric fields towards that secondary minimum location. At the same time, a much smaller electrical signal change would be expected when an analyte moves towards the center of the trap and away from the Au tips, because the plasmon-induced charge equilibration effect would be weaker. A much weaker electrical perturbation is indeed seen in Fig. 5b. Lastly, for the remaining ~14% of cases where no small optical step was detectable, we hypothesize that this was either due to noise or because the molecule entered directly into a stably-trapping hotspot and stayed there until it escaped.

6. LIMITATIONS OF THE CURRENT STUDY AND FUTURE WORK

During analysis of the phase data, namely Δφ and the Δφ gradient, we discovered that there was a prominent phase velocity component that overshadowed the small phase features we expected and Kitta et al.[16] investigated. We recognize there will be an inherent Δφ present in any filter and amplifier and in previous work, we found there was a frequency-dependent phase response from the sensor.[11] However, a step change in Δφ was reported to occur during translocation through a nanopore and was measured to be in the tens of mill-degrees.[16] Step changes of this magnitude were too small to detect using the analyses described above. In future work, we will use a lock-in amplifier, as was done by Kitta et al. [16] to isolate those small changes in Δφ, which will provide an additional AC frequency-dependent data type to characterize analytes. We plan on using a low-noise high-bandwidth amplifier (Elements Inc.), instead of the Axopatch 200B that is bandwidth-limited at 100 kHz, to test whether we can isolate the small amplitude Δφ features over a broader range of frequencies.

Furthermore, the present work only analyzed trap-initiation events, but no steady-state trapping or trap-escape conditions. In future work we will fit a sine wave to three regions for each trapping event namely, pre-trap, during and post-trap, to compare the phase shifts occurring in each condition. Our current work analyzed electrical signals in their totality. The HHT decomposes signals into intrinsic mode functions (IMFs) which, if used in future analysis, could reduce random noise contributions and provide further insights.

Finally, in our present setup, the electrode is placed at the entrance to a microfluidic channel on a coverslip, which is at a large distance (~100 μm) relative to the size of the nanosensor. This relatively large separation invites the question of whether the recorded electrical phase responses contained a component originating from other analytes in the vicinity of the nanosensor, but not at the center of the nanosensor. We are exploring options to add solid state electrodes to the sensor that will bring the electrodes within a few microns of the pore to mitigate this possible signal contamination.

7. CONCLUSION

This work presents preliminary results on the use of constant AC modulation as a means of identifying additional parameters to help differentiate between disparate analytes relative to DC data alone. The measurements were performed with a plasmonic nanopore that provided concurrent optical and electrical data, which helped further elucidate the analyte dynamics at the sensor by offering secondary features related to the movement of analytes inside the optical trap. These initial studies suggest that having constant AC modulation, superimposed to a DC voltage, may be advantageous because it provides a snapshot of instantaneous electrical responses as the analyte crosses the optical trap boundary. These early measurements indicate the possibility of improved separation between individual analytes and the complexes that they form compared to data previously obtained for AC modulation occurring during trapping.[11] It is possible that the transition into the optical trap creates higher amplitude electrical signal perturbations of different frequencies that could better differentiate analytes compared to corresponding measurements of AC modulation during trapping, where perturbation amplitudes are milder. Future work is needed to amass and aggregate more data to test the statistical significance of these hypotheses.

ACKNOWLEDGMENTS

We thank Dr. Karren L. More and Dr. Alex Belianinov for allowing us access and providing technical guidance on focused ion beam milling at the Center for Nanophase Materials Sciences (CNMS) at Oak Ridge National Laboratory (ORNL) in Oak Ridge, TN. We are also thankful to all the engineers and staff at the Shimadzu Institute Nanotechnology Research Center at the University of Texas at Arlington for their support and guidance. The authors acknowledge the financial support from the National Cancer Institute (1R21CA240220-01A1), the National Heart, Lung, and Blood Institute (NIH T32 HL134613) for Scott Renkes and the National Science Foundation (CBET#2022398 and CBET#2022374). The content is solely the responsibility of the authors and does not necessarily represent the official views of the National Institutes of Health.

REFERENCES

[1] Lu, Y., Wu, X.-Y., Ying, Y.-L. and Long, Y.-T., "Simultaneous single-molecule discrimination of cysteine and homocysteine with a protein nanopore," Chem. Commun. **55**(63), 9311–9314 (2019).

[2] Jain, M., Olsen, H. E., Paten, B. and Akeson, M., "The Oxford Nanopore MinION: delivery of nanopore sequencing to the genomics community," Genome Biol **17**(1), 239 (2016).

[3] Lee, J. S., Oviedo, J. P., Bandara, Y. M. N. D. Y., Peng, X., Xia, L., Wang, Q., Garcia, K., Wang, J., Kim, M. J. and Kim, M. J., "Detection of nucleotides in hydrated ssDNA via 2D h-BN nanopore with ionic-liquid/salt–water interface," ELECTROPHORESIS **42**(7–8), 991–1002 (2021).

[4] Nehra, A., Ahlawat, S. and Singh, K. P., "A biosensing expedition of nanopore: A review," Sensors and Actuators B: Chemical **284**, 595–622 (2019).

[5] Lee, J. S., Saharia, J., Bandara, Y. M. N. D. Y., Karawdeniya, B. I., Goyal, G., Darvish, A., Wang, Q., Kim, M. J. and Kim, M. J., "Stiffness measurement of nanosized liposomes using solid-state nanopore sensor with automated recapturing platform," ELECTROPHORESIS **40**(9), 1337–1344 (2019).

[6] Raza, M. U., Peri, S. S. S., Ma, L.-C., Iqbal, S. M. and Alexandrakis, G., "Self-induced back action actuated nanopore electrophoresis (SANE)," Nanotechnology **29**(43), 435501 (2018).

[7] Verschueren, D., Shi, X. and Dekker, C., "Nano-Optical Tweezing of Single Proteins in Plasmonic Nanopores," Small Methods **3**(5), 1800465 (2019).

[8] Al Balushi, A. A. and Gordon, R., "Label-free free-solution single-molecule protein–small molecule interaction observed by double-nanohole plasmonic trapping," ACS Photonics **1**(5), 389–393 (2014).

[9] Peri, S. S. S., Sabnani, M. K., Raza, M. U., Ghaffari, S., Gimlin, S., Wawro, D. D., Lee, J. S., Kim, M. J., Weidanz, J. and Alexandrakis, G., "Detection of specific antibody-ligand interactions with a self-induced back-action actuated nanopore electrophoresis sensor," Nanotechnology **31**(8), 085502 (2019).

[10] Peri, S. S. S., Sabnani, M. K., Raza, M. U., Urquhart, E. L., Ghaffari, S., Lee, J. S., Kim, M. J., Weidanz, J. and Alexandrakis, G., "Quantification of low affinity binding interactions between natural killer cell inhibitory receptors and targeting ligands with a self-induced back-action actuated nanopore electrophoresis (SANE) sensor," Nanotechnology **32**(4), 045501 (2020).

[11] Renkes, S., Kim, M. and Alexandrakis, G., "Label-free alternating-current plasmonic nanopore sensing of nanoparticles," Plasmonics in Biology and Medicine XIX **11978**, 53–62, SPIE (2022).

[12] Renkes, S., Peri, S. S. S., Raza, M. U., Weidanz, J., Kim, M. J. and Alexandrakis, G., "Self-induced Back-Action Actuated Nanopore Electrophoresis (SANE) Sensing," [Single Molecule Sensing Beyond Fluorescence], W. Bowen, F. Vollmer, and R. Gordon, Eds., Springer International Publishing, Cham, 389–412 (2022).

[13] Chen, Y., Kotnala, A., Yu, L., Zhang, J. and Gordon, R., "Wedge and gap plasmonic resonances in double nanoholes," Opt. Express **23**(23), 30227 (2015).

[14] van Hall, T., van de Rhee, N. E., Schoenberger, S. P., Vierboom, M. P., Verreck, F. A., Melief, C. J. and Offringa, R., "Cryptic open reading frames in plasmid vector backbone sequences can provide highly immunogenic cytotoxic T-lymphocyte epitopes," Cancer research **58**(14), 3087–3093 (1998).

[15] Verma, B., Jain, R., Caseltine, S., Rennels, A., Bhattacharya, R., Markiewski, M. M., Rawat, A., Neethling, F., Bickel, U. and Weidanz, J. A., "TCR mimic monoclonal antibodies induce apoptosis of tumor cells via immune effector-independent mechanisms," The Journal of Immunology **186**(5), 3265–3276 (2011).

[16] Kitta, K., Sakamoto, M., Hayakawa, K., Nukazuka, A., Kano, K. and Yamamoto, T., "Nanopore Impedance Spectroscopy Reveals Electrical Properties of Single Nanoparticles for Detecting and Identifying Pathogenic Viruses," ACS Omega **8**(16), 14684–14693 (2023).

[17] Asadzadeh, H., Renkes, S., kIM, M. and Alexandrakis, G., "Multi-Physics Simulations and Experimental Comparisons for the Optical and Electrical Forces Acting on a Silica Nanoparticle Trapped by a Double-Nanohole Plasmonic Nanopore Sensor," SSRN Scholarly Paper 4516042 (2023).

[18] Neumeier, L., Quidant, R. and Chang, D., "Self-induced back-action optical trapping in nanophotonic systems" (2015).